

Pseudo-giant number fluctuations and nematic order in microswimmer suspensions

Ismail El Korde,¹ Dóra Bárdfalvy,¹ Jason M. Lewis,¹ Alexander Morozov,² Cesare Nardini,^{3,4} and Joakim Stenhammar^{1,*}

¹*Division of Physical Chemistry, Lund University, P.O. Box 124, S-221 00 Lund, Sweden*

²*School of Physics and Astronomy, The University of Edinburgh, James Clerk Maxwell Building, Peter Guthrie Tait Road, Edinburgh, EH9 3FD, United Kingdom*

³*Service de Physique de l'État Condensé, CNRS UMR 3680, CEA-Saclay, 91191 Gif-sur-Yvette, France*

⁴*Sorbonne Université, CNRS, Laboratoire de Physique Théorique de la Matière Condensée, LPTMC, F-75005 Paris, France.*

(Dated: March 25, 2025)

Giant number fluctuations (GNFs), whereby the standard deviation ΔN in the local number of particles $\langle N \rangle$ grows faster than $\sqrt{\langle N \rangle}$, are a hallmark property of dry active matter systems with orientational order, such as a collection of granular particles on a vibrated plate. This contrasts with momentum-conserving (“wet”) active matter systems, such as suspensions of swimming bacteria, where no theoretical prediction of GNFs exist, although numerous experimental observations of such enhanced fluctuations have been reported. In this Letter, we numerically confirm the emergence of super-Gaussian number fluctuations in a 3-dimensional suspension of pusher microswimmers undergoing a transition to collective motion. These fluctuations emerge sharply above the transition, but only for sufficiently large values of the bacterial persistence length $\ell_p = v_s/\lambda$, where v_s is the bacterial swimming speed and λ the tumbling rate. Crucially, these “pseudo-GNFs” differ from true GNFs, as they only occur on length scales shorter than the typical size ξ of nematic patches in the collective motion state, which is in turn proportional to the single-swimmer persistence length ℓ_p . Our results thus suggest that observations of enhanced density fluctuations in biological active matter systems actually represent transient effects that decay away beyond mesoscopic length scales, and raises the question to what extent “true” GNFs with universal properties can exist in the presence of fluid flows.

Collective motion in active matter typically arises due to the coupling between activity, usually in the form of self-propulsion, and orientational (polar or nematic) order [1]. One generic feature of orientationally ordered flocks is the emergence of anomalously large, (*i.e.*, larger than Gaussian) fluctuations in the particle density, so-called giant number fluctuations (GNFs), whereby the standard deviation ΔN in the local number of particles N grows as $\langle N \rangle^\alpha$ with $\alpha > 1/2$ [2]. Experimentally, the emergence of GNFs in dry active matter was first demonstrated in a collection of rods on a vibrating plate [3], where collective motion arises from the coupling between activity-driven particle currents and (quasi-)long range order caused by particle collisions, and has since then been experimentally [4, 5] and numerically [6, 7] verified multiple times in both nematic and polar flocks. As we will demonstrate in this Letter, the situation in momentum-conserving, “wet”, active systems is however significantly different.

The emergence of GNFs in dry flocks can be understood by calculating the autocorrelation of density fluctuations in the orientationally ordered state [8, 9]. In the nematic case, the ensuing analysis shows that, at linear level, the variance $\langle \delta n(\mathbf{q}, t) \delta n(-\mathbf{q}, t) \rangle$ in the local number density n of the ordered flock diverges as q^{-2} for small $q = |\mathbf{q}|$, which, in 2 dimensions, yields a linear growth of ΔN with $\langle N \rangle$, *i.e.*, $\alpha = 1$. This picture is changed when accounting for the effect of non-linearities [10], which lead to non-universal exponents that depend on the microscopic model parameters.

In wet active matter, the situation is even more complex: Since the nematically ordered state is generically unstable for finite wavenumbers in the presence

of fluid flows [11], the route used in the dry case to calculate $\langle \delta n(\mathbf{q}, t) \delta n(-\mathbf{q}, t) \rangle$, based on a computation at linear level followed by the treatment of non-linearities within a renormalization group framework [8, 10], is no longer accessible. Therefore, no quantitative predictions exist for the emergence of GNFs in bulk wet active nematics, although they have been predicted for nematic flocks moving through a fluid in contact with a substrate which stabilises the orientationally ordered state [12]. There are however numerous experimental [13–17] (and some numerical [18]) observations of enhanced concentration fluctuations in various biological incarnations of wet active matter, suggesting that such fluctuations are indeed a common feature in the presence of momentum conservation as well. Due to experimental limitations, is however difficult to assess whether these observations represent “true” GNFs with asymptotically valid power laws with associated universal exponents, or merely transient effects where fluctuations appear non-Gaussian because distributional convergence has not yet been reached.

The archetypical example of collective motion in wet active matter is the transition to so-called bacterial turbulence in dilute suspensions of rear-actuated, “pusher” microorganisms such as *E. coli* and *B. subtilis* [19–22]. In a 3-dimensional, unbounded suspension of pusher microswimmers at density n , this transition is predicted to occur for [23–25]

$$n > n_c^\infty = \frac{5\lambda}{\kappa}, \quad (1)$$

where κ is the dipole strength, with $\kappa > 0$ corresponding to pushers, and λ is the rate of bacterial reorientation (“tumbles”). The critical number density in Eq. (1)

represents the long-wavelength destabilisation of the homogeneous and isotropic suspension caused by bacterial reorientation due to flow alignment. Since the dipolar flow field is fully fore-aft symmetric, the ensuing orientationally ordered state exhibits nematic symmetry; however this state in turn immediately destabilises due to the presence of fluid flows [11], leading to a highly nonlinear, turbulent state characterised by short-ranged nematic order and long-range chaotic flows [23, 26]. The fore-aft symmetry of the system is broken by the presence of self-propulsion, whereby each swimmer moves along its director \mathbf{p} with constant speed v_s . Crucially, however, v_s does *not* affect the mean-field critical density in (1) [27]; this observation is far from trivial, as exemplified by the emergence of collective motion near a confining boundary, where v_s enters the expression for n_c even at mean-field level [28, 29]. In unbounded suspensions, v_s instead enters when including the effect of correlations, where swimming acts to suppress pretransitional swimmer-swimmer correlations for $n < n_c$ [27].

In this Letter, we numerically confirm the experimental observation that super-Gaussian number fluctuations occur generically above the transition to collective motion in microswimmer suspensions. Unlike in dry active systems, however, these only occur on length scales small enough compared to the bacterial persistence length $\ell_p = v_s/\lambda$, beyond which number fluctuations start to decay towards the expected Gaussian behaviour. By analysing the range of orientational order in the collective motion regime, we show that the size ξ of nematic patches is also proportional and comparable to ℓ_p , thus establishing a direct link between nematic order and non-Gaussian number fluctuations in momentum-conserving active systems. Our results therefore demonstrate that true GNFs, in the sense of being a large-scale property exhibiting universal exponents, are suppressed in the presence of fluid flow, providing a new perspective on previous experimental observations of anomalous number fluctuations in wet active systems [13–17].

We consider a dilute, 3-dimensional suspension of pusher microswimmers at nominal number density n moving through an incompressible, viscous fluid with viscosity μ and mass density ρ . Each swimmer is modeled as an extended force dipole of magnitude $\kappa = F\ell/\mu$ acting on the fluid, with F the force magnitude and ℓ the dipole length. The position \mathbf{r}_i and orientation \mathbf{p}_i of swimmer i evolve according to

$$\dot{\mathbf{r}}_i = v_s \mathbf{p}_i + \mathbf{U}(\mathbf{r}_i), \quad (2)$$

$$\dot{\mathbf{p}}_i = (\mathbb{I} - \mathbf{p}_i \mathbf{p}_i) \cdot \nabla \mathbf{U}(\mathbf{r}_i) \cdot \mathbf{p}_i, \quad (3)$$

where $\mathbf{U}(\mathbf{r}_i)$ is fluid velocity measured at the position of the swimmer body, v_s is the (constant) swimming speed, and \mathbb{I} is the unit tensor. In addition to the rotation by the ambient fluid described by (3), each swimmer randomises its swimming direction (“tumbles”) with average frequency λ .

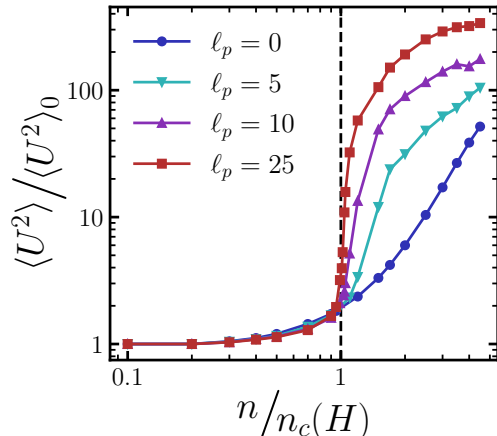


Figure 1. Fluid velocity variance $\langle U^2 \rangle$ normalised by its corresponding value in a non-interacting suspension, $\langle U^2 \rangle_0$, for various values of the swimmer persistence length ℓ_p . The microswimmer density n is normalised by the critical density $n_c(H)$ from Eqs. (1) and (4). Note that increasing the swimming speed, measured through ℓ_p , sharpens the transition by suppressing pretransitional swimmer-swimmer correlations.

The temporal evolution of the flow field $\mathbf{U}(\mathbf{r}, t)$ was solved using a point-force implementation of the lattice Boltzmann (LB) algorithm described previously [25, 26, 30, 31], using a cubic box of linear size H with periodic boundaries. In terms of LB units, defined by the lattice spacing ΔL and the time step Δt , the swimmer parameters were set to $F = 1.57 \times 10^{-3}$, $\ell = 1$, roughly corresponding to the value of κ measured for *E. coli* [26, 32], and $\lambda = 2 \times 10^{-4}$. We furthermore set $\mu = 1/6$, corresponding to full relaxation of the fluid to local equilibrium at each timestep, and $\rho = 1$. The average persistence length $\ell_p = v_s/\lambda$, was controlled by varying the swimming speed v_s between zero and 5×10^{-3} while keeping λ constant. Unless otherwise stated, results are presented for a system size $H = 100$. In the following, all lengths are expressed in terms of the swimmer length ℓ .

We begin by characterising the transition from disordered swimming to collective motion, and in particular the effect of varying the swimming speed v_s . As an order parameter, we choose the reduced space- and time-averaged fluid velocity variance, $\langle U^2 \rangle / \langle U^2 \rangle_0$, where $\langle U^2 \rangle_0$ is the corresponding value measured in suspension of non-interacting microswimmers. In Fig. 1, we plot this quantity as a function of the reduced microswimmer density $n/n_c(H)$, where $n_c(H)$ is the analytically known critical density in a finite system of linear size H [33]:

$$n_c(H) = n_c^\infty \left[1 + \frac{3\pi}{5} \frac{\ell_p}{H} + \frac{4\pi^2}{5} \left(\frac{\ell_p}{H} \right)^2 \right], \quad (4)$$

with n_c^∞ given by Eq. (1). Equation (4) encodes the fact that the mean-field hydrodynamic instability leading to bacterial turbulence occurs at the longest length-scale available, which, in a system of linear size H ,

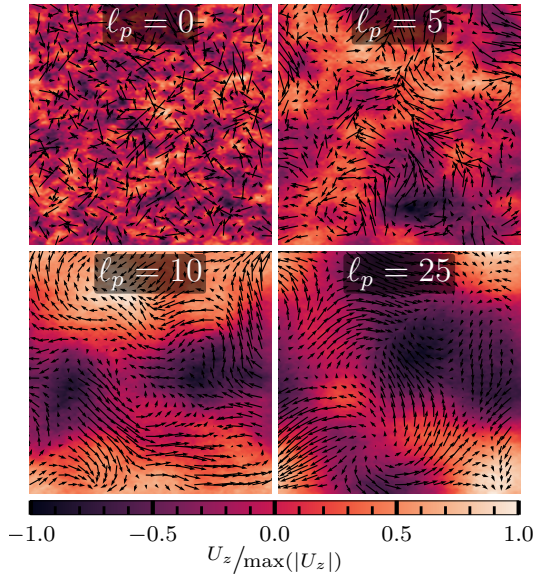


Figure 2. Snapshots of a $2d$ slice of the $3d$ flow field for $n/n_c = 2.0$ and $H = 250$, for the values of l_p indicated. Arrows show the in-plane component and colours show the out-of-plane component of \mathbf{U} , scaled by its maximum value.

corresponds to a critical wave vector $k_c = 2\pi/H$. Using this correction, the results in Fig. 1 confirm the theoretical prediction from [27] that faster swimming effectively sharpens the transition to collective motion without shifting the critical density by suppressing pre-transitional swimmer-swimmer correlations. Crucially, this sharpening is thus *not* a finite-size effect: As we show in [34] (see also [25, 26]), increasing H does not lead to a sharpening of the transition, unlike what one would expect from a critical phase transition. The analysis in Fig. 1 also shows that the theoretically predicted critical density given by Eqs. (1) and (4) coincides with the numerically observed, sharp increase in $\langle U^2 \rangle$. Even though the instability encoded in Eq. (1) has been numerically studied numerous times using both continuum [23] and particle-resolved [18, 26] simulations, the results in Fig. 1 to our knowledge constitute the first quantitative verification of this prediction. The snapshots in Fig. 2 visually confirm a strong effect of l_p also on the properties of the turbulent state: For shakers ($l_p = 0$), the flow field appears almost random with very short-ranged correlations, while faster swimming, and thus larger l_p , leads to increasingly large-scale flow structures appearing in the velocity field. Importantly, as we show below, this effect on the flow field is likewise reflected as an increase in the typical range of swimmer orientational order with l_p .

To quantify the emergence of non-Gaussian number fluctuations at the transition to collective motion, we first consider the spatiotemporal average $\langle N \rangle$ and the corresponding standard deviation ΔN of the number of particles in randomly sampled spherical volumes of varying radius R . For $n > n_c$ and $l_p > 0$, it is clear from the results in Fig. 3a that

ΔN grows faster than $\sqrt{\langle N \rangle}$, indicating the emergence of GNFs in the collective motion state. For shakers ($l_p = v_s = 0$), no such enhanced fluctuations are seen, which, as was first noted by Saintillan and Shelley [35], is a consequence of the fact that the local polar order which drives density fluctuations is strictly zero for shakers, since there is no term in the microscopic equations of motion that break fore-aft symmetry. For finite l_p , $\Delta N/\sqrt{\langle N \rangle}$ has a non-monotonic behaviour, with significantly enhanced number fluctuations for small and intermediate $\langle N \rangle$, followed by a fast decrease for larger $\langle N \rangle$. This behaviour is qualitatively similar to previous experimental [3–5, 13, 15–17] and numerical [6, 7] observations of GNFs, and can partially be explained by the unavoidable damping of number fluctuations at large length scales due to global particle conservation; as we will see in the following, this is however not the primary mechanism at work here. That the underlying physics is more complex than just mass conservation is already visible from the two curves for $l_p = 5$ in Fig. 3a and b: These show that increasing the system size from $H = 100$ to $H = 250$ does *not* extend the region of enhanced number fluctuations as expected for true GNFs, but rather leads to the development of an intermediate plateau with Gaussian fluctuations preceding the decay due to finite H .

Due to the difficulty in consistently fitting a power-law to the very limited data range, in Fig. 3b we instead approximate the derivative $d \log \Delta N / d \log \langle N \rangle$ by differentiating a high-order polynomial fitted to the data in Fig. 3a. From this data, we operationally define the *apparent* GNF exponent α_{app} as the maximum in $d \log \Delta N / d \log \langle N \rangle$, located at $R \equiv R^*$, as shown in Fig. 3b. Based on this analysis, in Fig. 3c we plot α_{app} as a function of the microswimmer density, clearly verifying the sharp onset of non-Gaussian concentration fluctuations at $n = n_c$; for large l_p , α_{app} in fact appears to provide an even clearer measure of the transition point than the velocity variance (Fig. 1). Even given the limitations of its operational definition, it is clear that α_{app} does not approach any universal value, as it depends strongly on both l_p and on n , with a maximum slightly above n_c . Unsurprisingly, α_{app} also exhibits strong finite size effects, although it asymptotes to a characteristic value for each l_p as H becomes sufficiently large [34].

To investigate the origin of the non-monotonic behaviour in Fig. 3a, in Fig. 3d we plot R^* , which characterises the length scale at which density fluctuations are maximised, as a function of the system size H . For true GNFs, one expects the region where non-Gaussian fluctuations are observed to grow in an unbounded fashion with H , approaching a universal power-law in the thermodynamic limit. Here, R^* instead exhibits an initial increase until it saturates at $R^* \approx 0.8l_p$ for $H \approx 20l_p$. (The suboptimal data collapse for $l_p = 15$ is an inertial effect, which we discuss further below.) This analysis clearly shows that

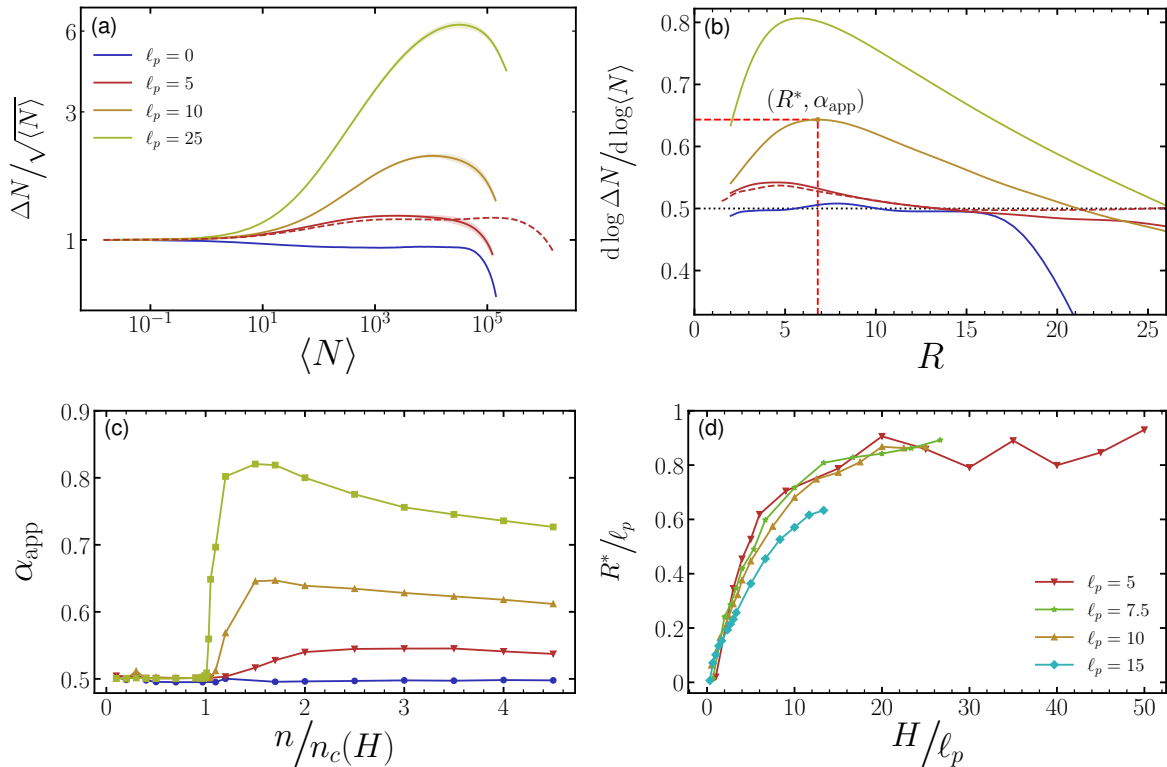


Figure 3. (a) Reduced standard deviation $\Delta N / \sqrt{\langle N \rangle}$ of the average number of particles N in a spherical volume as a function of $\langle N \rangle$ obtained for $n/n_c = 2.0$ and various ℓ_p , as indicated. The dashed line for $\ell_p = 5$ shows the same quantity for a larger system size, $H = 250$, showing the development of an extended plateau of Gaussian fluctuations for intermediate length scales. The shaded area denotes one standard deviation, estimated by averaging each run over ten sub-batches. (b) The derivative $d \log \Delta N / d \log \langle N \rangle$ plotted as a function of the radius R of the sampling volume. The maximum in $d \log \Delta N / d \log \langle N \rangle$ defines the apparent GNF exponent α_{app} , and its location defines R^* . (c) α_{app} as a function of the reduced microswimmer density n/n_c . Notice that non-Gaussian fluctuations emerge at the transition to collective motion only for sufficiently large ℓ_p and are completely absent for shakers. (d) R^*/ℓ_p as a function of the reduced system size H/ℓ_p for $n/n_c = 2.0$. The data collapse shows that, for sufficiently large system sizes $H \gg \ell_p$, R^* is controlled by ℓ_p ; hence, the apparently non-Gaussian fluctuations are only transient.

the non-Gaussian fluctuations which emerge above n_c are not “true” GNFs in the sense of being a universal property that survives in the thermodynamic limit, but rather “pseudo-GNFs” that occur transiently over mesoscopic length scales. These results establish that R^* is directly proportional to ℓ_p above the transition to collective motion, although their relationship contains a density-dependent prefactor which we expect to remain close to unity reasonably far above n_c .

In dry active systems, GNFs arise due to the coupling between (quasi-)long range orientational order and non-equilibrium dynamics [2, 8]. In the presence of a fluid, the emergent, orientationally ordered state encoded in the instability criterion of Eq. (1) is however unstable for finite wavenumbers [11], resulting in the chaotic motion that is characteristic of the turbulent state. To establish a connection between local nematic order and the pseudo-GNFs established in Fig. 3, we calculate the distance-dependent, scalar swimmer-swimmer nematic order $S(r) \equiv \frac{1}{2} \langle 3 \cos^2 \theta - 1 \rangle_r$, where θ is the angle formed between the two swimmer orientation vectors and $\langle \dots \rangle_r$ denotes a spatiotempo-

ral average over all swimmer pairs with a given separation r . For $\ell_p = 0$, we find that $S(r)$ is well fitted by a stretched exponential, $S(r) = S_0 e^{-(r/\xi)^\beta}$ with $\beta \geq 1$ and a single decay length ξ [34]. For $\ell_p > 0$, $S(r)$ has a complex shape with no obvious analytical description [26], and we therefore instead fit the initial decay of $S(r)$ using a regular exponential form, $S(r) = S_0 e^{-r/\xi}$ [34]. In spite of this complexity, for both shakers and swimmers it is natural to interpret ξ as the characteristic size of nematic patches in the turbulent state. In Fig. 4a we show the extracted values of ξ as a function of n/n_c for the same parameter set as in Fig. 3c. Even though the jump in ξ at $n = n_c$ is less sharp than for α_{app} , the similarity between the two datasets is striking, and it is clear that the onset of collective motion for large ℓ_p is characterised by a sharp increase in the range of nematic order. In Fig. 4b we further plot ξ as a function of ℓ_p for $n/n_c = 2.0$ and four different system sizes H . Even though the finite-size effects are large, the four datasets all present the same linear scaling of ξ on ℓ_p , although the large- ℓ_p behaviour is likely also some-

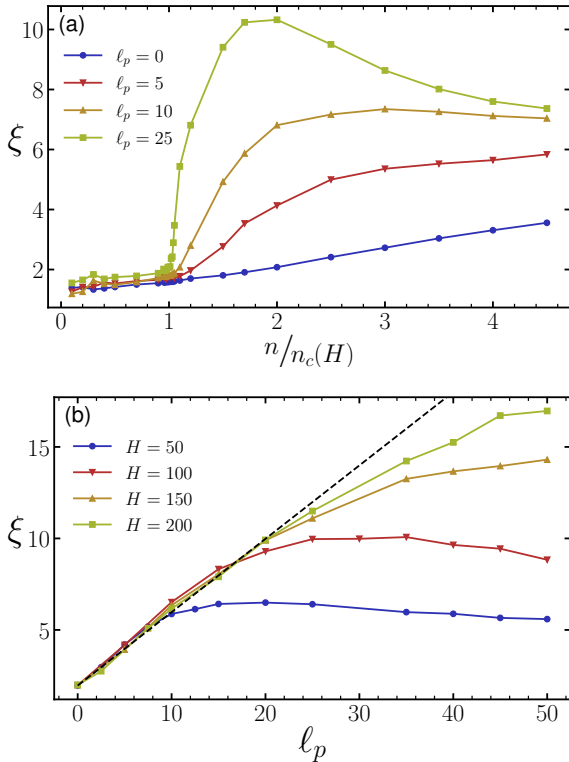


Figure 4. (a) Fitted values of the nematic length-scale ξ as a function of the reduced microswimmer density for $H = 100$ and various ℓ_p , as indicated. Notice the similarity with the data in Fig. 3c. (b) ξ plotted as a function of ℓ_p for $n/n_c = 2.0$ and four different values of H , as indicated. The dashed line shows a linear fit to the first six data points for $H = 200$.

what affected by swimmer inertia, as discussed below. This result strongly suggests that the size of nematic patches in an unbounded system at a given $n/n_c > 1$ is directly controlled by ℓ_p , in accordance with previous findings [26]. This finding might initially seem surprising, since the most unstable wave-number of the homogeneous and isotropic state encoded in Eq. (4) corresponds to the largest available length-scale in the system [28]. However, ξ is more likely controlled by the smallest stable wavenumber of the *nematic* state, which we expect to set the maximum size of stable nematic patches in the turbulent state. Starting from a continuum description of the suspension in terms of the density and nematic order [35, 36], it can indeed be shown via dimensional analysis that the maximum size of stable nematic patches when $n > n_c$ is finite and increases linearly with ℓ_p to leading order.

The results presented in this Letter thus establish a clear connection between (i) the characteristic length scale over which non-Gaussian concentration fluctuations are observed, as encoded in R^* , and (ii) the size of nematic patches in the turbulent regime, as encoded in ξ . We observe that number fluctuations inside a nematic patch grow until reaching $R^* \approx \xi$, where the latter length scale is selected by the largest stable length scale of a nematically ordered state in the presence

of fluid flows [8]. At scales much larger than ξ , the orientational correlations between individual patches vanish [26], restoring Gaussian fluctuations as in equilibrium. Therefore, our results clearly establish that the non-Gaussian number fluctuations observed in our model do not constitute an example of GNFs in the universal sense, which is a direct consequence of the absence of a stable, nematically ordered state. Since this instability is generic in the presence of fluid flows and occurs for arbitrary values of activity, whether extensile or contractile [11], our results suggest that true GNFs are in fact *generically* absent from wet active systems with nematic alignment.

Remarkably, both ξ and R^* are directly proportional to the microscopic persistence length ℓ_p , showing that, even though v_s is absent from the instability criterion in Eq. (1), swimming has a profound effect on the properties of both the pretransitional suspension [27] and the turbulent state itself. Since $R^* \sim \xi \sim \ell_p$, there exists a possibility of restoring universal GNFs in the limit $\ell_p \rightarrow \infty$: Because α_{app} is strictly bounded by unity, corresponding to a maximally segregated system, the results in Fig. 3 suggest that, for sufficiently large ℓ_p and $H \gg \ell_p$, one might recover an extended power-law region with a universal exponent. Extending the numerics to larger ℓ_p is however computationally prohibitive, for two reasons: First of all, reaching $H \gg \ell_p$ requires massive system sizes, which limits the data range in Fig. 3d. Secondly, since the LB method intrinsically operates at finite Reynolds number, increasing v_s eventually leads to non-negligible effects of swimmer inertia, which become significant for $\text{Re} \equiv v_s \ell_p \rho / \mu \geq 0.1$ [30, 37]. For the current parameter set, this translates to $\ell_p \geq 9$, in agreement with the observed decline in the data collapse in Fig. 3d. An alternative approach is a field-theoretical treatment of the emergence of non-Gaussian fluctuations, similar to the strategy used in the dry case [8–10]. A straightforward translation of this approach to wet systems is however not possible even at linear level, as it relies on the long-wavelength perturbation of a stable, nematically ordered base state, which is absent in the presence of fluid flows.

Regardless of whether true GNFs are formally recovered in the $\ell_p \rightarrow \infty$ limit, our data clearly establish that GNFs in the universal sense cannot not be generically expected under physically realistic conditions in wet active systems with underlying nematic order. Our results thus provide a new perspective on observations of non-Gaussian fluctuations in biological realisations of active matter [13–17] as well as novel insights into the factors that control the emergent properties of collective motion in bacterial suspensions.

Acknowledgements. Helpful discussions with Sriram Ramaswamy and Ananyo Maitra are kindly acknowledged. JS acknowledges funding from the Knut and Alice Wallenberg Foundation (grant 2019.0079).

-
- * joakim.stenhammar@fkem1.lu.se
- [1] M. C. Marchetti, J. F. Joanny, S. Ramaswamy, T. B. Liverpool, J. Prost, M. Rao, and R. A. Simha, Hydrodynamics of soft active matter, *Rev. Mod. Phys.* **85**, 1143 (2013).
- [2] S. Ramaswamy, The mechanics and statistics of active matter, *Annu. Rev. Fluid Mech.* **1**, 323 (2010).
- [3] V. Narayan, S. Ramaswamy, and N. Menon, Long-lived giant number fluctuations in a swarming granular nematic, *Science* **317**, 105 (2007).
- [4] N. Kumar, H. Soni, S. Ramaswamy, and A. K. Sood, Flocking at a distance in active granular matter, *Nat. Commun.* (2014).
- [5] J. Deseigne, O. Dauchot, and H. Chaté, Collective motion of vibrated polar disks, *Phys. Rev. Lett.* **105**, 098001 (2010).
- [6] H. Chaté, F. Ginelli, and R. Montagne, Simple model for active nematics: Quasi-long-range order and giant fluctuations, *Phys. Rev. Lett.* **96**, 180602 (2006).
- [7] H. Chaté, F. Ginelli, G. Grégoire, and F. Raynaud, Collective motion of self-propelled particles interacting without cohesion, *Phys. Rev. E* **77**, 046113 (2008).
- [8] S. Ramaswamy, R. A. Simha, and J. Toner, Active nematics on a substrate: Giant number fluctuations and long-time tails, *Europhys. Lett.* **62**, 196 (2003).
- [9] J. Toner, Giant number fluctuations in dry active polar fluids: A shocking analogy with lightning rods, *J. Chem. Phys.* **150**, 154120 (2019).
- [10] S. Shankar, S. Ramaswamy, and M. C. Marchetti, Low-noise phase of a two-dimensional active nematic system, *Phys. Rev. E* **97**, 012707 (2018).
- [11] R. A. Simha and S. Ramaswamy, Hydrodynamic fluctuations and instabilities in ordered suspensions of self-propelled particles, *Phys. Rev. Lett.* **89**, 058101 (2002).
- [12] A. Maitra, P. Srivastava, M. C. Marchetti, J. S. Lintuvuori, S. Ramaswamy, and M. Lenz, A nonequilibrium force can stabilize 2D active nematics, *Proc. Natl. Acad. Sci.* **115**, 6934 (2018).
- [13] Z. Liu, W. Zeng, X. Ma, and X. Cheng, Density fluctuations and energy spectra of 3D bacterial suspensions, *Soft Matter* **17**, 10806 (2021).
- [14] G. Duclos, S. Garcia, H. G. Yevick, and P. Silberzan, Perfect nematic order in confined monolayers of spindle-shaped cells, *Soft Matter* **10**, 2346 (2014).
- [15] D. Nishiguchi, K. H. Nagai, H. Chaté, and M. Sano, Long-range nematic order and anomalous fluctuations in suspensions of swimming filamentous bacteria, *Phys. Rev. E* **95**, 020601 (2017).
- [16] F. Peruani, J. Starruß, V. Jakovljevic, L. Søgaard-Andersen, A. Deutsch, and M. Bär, Collective motion and nonequilibrium cluster formation in colonies of gliding bacteria, *Phys. Rev. Lett.* **108**, 098102 (2012).
- [17] H. P. Zhang, A. Be'er, E.-L. Florin, and H. L. Swinney, Collective motion and density fluctuations in bacterial colonies, *Proc. Natl. Acad. Sci.* **107**, 13626 (2010).
- [18] D. Saintillan and M. J. Shelley, Emergence of coherent structures and large-scale flows in motile suspensions, *J. Royal Soc. Interface* **9**, 571 (2012).
- [19] J. Gachelin, A. Rousselet, A. Lindner, and E. Clément, Collective motion in an active suspension of *Escherichia coli* bacteria, *New J. Phys.* **16**, 025003 (2014).
- [20] A. Sokolov and I. S. Aranson, Physical properties of collective motion in suspensions of bacteria, *Phys. Rev. Lett.* **109**, 248109 (2012).
- [21] J. Dunkel, S. Heidenreich, K. Dreschner, H. H. Wensink, M. Bär, and R. E. Goldstein, Fluid dynamics of bacterial turbulence, *Phys. Rev. Lett.* **110**, 228102 (2013).
- [22] H. H. Wensink, J. Dunkel, S. Heidenreich, K. Drescher, R. E. Goldstein, H. Löwen, and J. M. Yeomans, Mesoscale turbulence in living fluids, *Proc. Natl. Acad. Sci. USA* **109**, 14308 (2012).
- [23] D. Saintillan and M. J. Shelley, Instabilities, pattern formation, and mixing in active suspensions, *Phys. Fluids* **20**, 123304 (2008).
- [24] D. Saintillan and M. J. Shelley, Orientational order instabilities in suspensions of self-locomoting rods, *Phys. Rev. Lett.* **99**, 058102 (2007).
- [25] J. Stenhammar, C. Nardini, R. W. Nash, D. Marenduzzo, and A. Morozov, Role of Correlations in the Collective Behaviour of Microswimmer Suspensions, *Phys. Rev. Lett.* **119**, 028005 (2017).
- [26] D. Bárdfalvy, H. Nordanger, C. Nardini, A. Morozov, and J. Stenhammar, Particle-resolved lattice Boltzmann simulations of 3-dimensional active turbulence, *Soft Matter* **15**, 7747 (2019).
- [27] V. Škultéty, C. Nardini, J. Stenhammar, D. Marenduzzo, and A. Morozov, Swimming suppresses correlations in dilute suspensions of pusher microorganisms, *Phys. Rev. X* **10**, 031059 (2020).
- [28] V. Škultéty, D. Bárdfalvy, J. Stenhammar, C. Nardini, and A. Morozov, Hydrodynamic instabilities in a two-dimensional sheet of microswimmers embedded in a three-dimensional fluid, *J. Fluid. Mech.* **980**, A28 (2024).
- [29] D. Bárdfalvy, V. Škultéty, C. Nardini, A. Morozov, and J. Stenhammar, Collective motion in a sheet of microswimmers, *Commun. Phys.* **7** (2024).
- [30] R. W. Nash, R. Adhikari, and M. E. Cates, Singular forces and pointlike colloids in lattice Boltzmann hydrodynamics, *Phys. Rev. E* **77**, 026709 (2008).
- [31] R. W. Nash, R. Adhikari, J. Tailleur, and M. E. Cates, Run-and-Tumble Particles with Hydrodynamics: Sedimentation, Trapping, and Upstream Swimming, *Phys. Rev. Lett.* **104**, 258101 (2010).
- [32] K. Drescher, J. Dunkel, L. H. Cisneros, S. Ganguly, and R. E. Goldstein, Fluid dynamics and noise in bacterial cell-cell and cell-surface scattering, *Proc. Natl. Acad. Sci.* **108**, 10940 (2011).
- [33] V. A. Martinez, E. Clément, J. Arlt, C. Douarche, A. Dawson, J. Schwarz-Linek, A. K. Creppy, V. Škultéty, A. N. Morozov, H. Auradou, and W. C. K. Poon, A combined rheometry and imaging study of viscosity reduction in bacterial suspensions, *Proc. Natl. Acad. Sci.* **117**, 2326 (2020).
- [34] See Supplemental Material at [URL to be inserted by publisher] for further details.
- [35] D. Saintillan and M. J. Shelley, Theory of active suspensions, in *Complex Fluids in Biological Systems: Experiment, Theory, and Computation*, edited by S. E. Spagnolie (Springer New York, New York, NY, 2015) pp. 319–355.
- [36] V. Škultéty, *Collective motion in microswimmer suspensions*, PhD Thesis, The University of Edinburgh (2023).
- [37] J. de Graaf and J. Stenhammar, Lattice-Boltzmann simulations of microswimmer-tracer interactions, *Phys. Rev. E* **95**, 023302 (2017).